

# Treatment of acute myeloid leukemia, acute lymphoblastic leukemia and acute T cell leukemia by Ag NP/chitosan-starch nano-biocomposite

Man Li<sup>1</sup>

<sup>1</sup>Harbin Medical University

October 31, 2022

## Abstract

We herein demonstrate the biogenic nanoarchitectonics of silver nanoparticles template over chitosan/starch mixed hydrogel having excellent reducing ability. The two biopolymers also had the capacity to stabilize as-synthesized Ag NPs. Physicochemical and structural features of the nanocomposite biomaterial was assessed by several techniques like FT-IR, SEM, TEM, EDX and XRD. TEM study revealed the mean diameter of the spherical shaped Ag NPs/CS-Starch material was in the range of 5-15 nm. Thereafter, the Ag NPs/CS-Starch bio-composite material was exploited in the study of cytotoxicity and anti-leukemia effects against diverse leukemia cell lines like acute myeloid leukemia (32D-FLT3-ITD and Human HL-60/vcr), acute lymphoblastic leukemia (MOLT-3 and TALL-104), and acute T cell leukemia (Jurkat, Clone E6-1 and J.RT3-T3.5) *in situ*. Interestingly, the nano-drug could resist significantly against those cell lines in a time and concentration-dependent manner, assessed by MTT method. The corresponding IC<sub>50</sub> values of the bio-composite were 203, 301, 250, 227, 102, and 193  $\mu\text{g}/\text{mL}$  respectively against the cell lines. Furthermore, antioxidant potential of the material was investigated by DPPH radical scavenging method. A significantly high IC<sub>50</sub> value suggested the high antioxidant capacity of Ag NPs/CS-Starch nanomaterial.

## Treatment of acute myeloid leukemia, acute lymphoblastic leukemia and acute T cell leukemia by Ag NP/chitosan-starch nano-biocomposite

Man Li\*

Department of Endoscopy, Harbin Medical University Cancer Hospital, Harbin, Heilongjiang, 150081, China, Pre-test triage, The Fourth People's Hospital of Jinan, Jinan city, China.

\* Corresponding author: dr.man.li.12345@gmail.com

**Abstract.** We herein demonstrate the biogenic nanoarchitectonics of silver nanoparticles template over chitosan/starch mixed hydrogel having excellent reducing ability. The two biopolymers also had the capacity to stabilize as-synthesized Ag NPs. Physicochemical and structural features of the nanocomposite biomaterial was assessed by several techniques like FT-IR, SEM, TEM, EDX and XRD. TEM study revealed the mean diameter of the spherical shaped Ag NPs/CS-Starch material was in the range of 5-15 nm. Thereafter, the Ag NPs/CS-Starch bio-composite material was exploited in the study of cytotoxicity and anti-leukemia effects against diverse leukemia cell lines like acute myeloid leukemia (32D-FLT3-ITD and Human HL-60/vcr), acute lymphoblastic leukemia (MOLT-3 and TALL-104), and acute T cell leukemia (Jurkat, Clone E6-1 and J.RT3-T3.5) *in situ*. Interestingly, the nano-drug could resist significantly against those cell lines in a time and concentration-dependent manner, assessed by MTT method. The corresponding IC<sub>50</sub> values of the bio-composite were 203, 301, 250, 227, 102, and 193  $\mu\text{g}/\text{mL}$  respectively against the cell lines. Furthermore, antioxidant potential of the material was investigated by DPPH radical scavenging method. A significantly high IC<sub>50</sub> value suggested the high antioxidant capacity of Ag NPs/CS-Starch nanomaterial.

**Keywords:** Chitosan-Starch, Silver nanoparticles, cytotoxicity, Leukemia, Antioxidant.

## 1. Introduction

In recent times, nanotechnology is an extremely emerging and developing field having tremendous implications both in academia and industry. A number of physical, chemical and biological methods have been adopted to formulate different kind of nanoparticles. The physical methods of preparation involve high pressure and temperature. The techniques are also quite expensive [1-4]. Also, in many chemical pathways, the chemicals used are very harmful and toxic to the environment as well as for biological systems. The by-products derived from the chemical methods are also very toxic. So, the need for a suitable cost-effective and efficient pathway that does not produce toxic substances, without affecting the environment is highly demanding [5,6]. Adoption of biological procedure is one of the best ways to solve the above discrepancies to the synthesis of nanoparticles. The mother nature has provided a great resource in this regard. Different microorganisms like bacteria, actinomycetes, fungi and algae as well as plants and plant extracts are employed as the biological template in the synthesis of nanoparticles [7-9]. Recently, plant extracts have been widely used in the synthesis of functionalized nanoparticles. The typical advantage in the phytosynthesis of nanoparticle using plant extracts are the use of water as only solvent, being essentially abundant, green and safe solvent. The nanoparticle biosynthesis using biological materials is also very simple and does not need special conditions that are required in chemical and physical ways [10-12]. The reduction potential of biological materials is higher than that of microbial culture media, and as a result, the time required for the nanoparticle formation is comparatively less. The pollution created during the nanoparticle biosynthesis using biological materials is almost zero. As a result, the nanoparticle biosynthesis using biological materials has very low environmental impact, highly compatible with the environment [9-11]. However, the speed of production, quality and other properties of nanoparticles depend on many factors such as the nature of biological materials, reaction time, temperature, pH, metal salt concentration, and extract concentration. The use of biological materials due to their environmental compatibility with the abundance are usually prioritized. Also, due to their lack of need for special nutrients and conditions for growth, biological materials are considered the best option for the nanoparticle production [7-10].

Nanoparticles are designed in such a way that they can carry a higher dose of medicine with them and deliver it to the target area that is affected by cancer. In fact, these particles are not a threat to healthy body cells and only affect cancer cells and destroy them [11-13]. This method is considered a targeted treatment that attacks only the target cells and acts selectively. By this method on several patients, positive and satisfactory results have been obtained, which can be considered as part of the great developments of medical science in the field of cancer treatment [10-14].

With these inputs, we wish to report herein a competent biogenic synthesis of bio-functionalized tiny Ag NPs templated over the chitosan-starch mixed polymeric hydrogel. The biopolymers facilitate the binding of incoming Ag ions followed by green reduction to the corresponding NPs. The polar electron rich organo functions (OH, CH<sub>2</sub>OH, NH<sub>2</sub>) prevailed over the conjugate biopolymers also helps in the stabilization of the as-synthesized NPs by encapsulation or capping and preventing them from self-agglomerations. Based on the structure oriented anti-cancer activities of different bio-functionalized nanoparticles, the Ag NPs/CS-Starch bio-composite nanomaterial was employed in the determination of cytotoxicity and anti-leukemina activities against a number of corresponding cell lines like acute myeloid leukemia (32D-FLT3-ITD and Human HL-60/vcr), acute lymphoblastic leukemia (MOLT-3 and TALL-104), and acute T cell leukemia (Jurkat, Clone E6-1 and J.RT3-T3.5). In all of them the % cell viability decreases dose-dependently. In addition, the material was studied in the determination of antioxidant properties through the well known DPPH radical scavenging analysis, which in turn showed outstanding activity, being referenced to BHT molecule.

## 2. Experimental

### 2.1. Preparation of the Ag NPs/CS-Starch bio-composite

At the outset the CS/starch mixed hydrogel was prepared by sonicating a mixture of chitosan (98% NH<sub>2</sub>) and starch (0.5 g each) in 100 mL of 1% (v/v) acetic acid followed by stirring overnight at room temperature.

Prior to addition of Ag precursor, it was then made alkaline to pH 9 by adding dilute NaOH. An aqueous solution of AgNO<sub>3</sub> (30 mg in 10 mL) was added very slowly and drop-wise to the hydrogel under ambient conditions and stirred for 2 h maintaining a temperature of 100 °C. Soon, the solution color changed from colorless to grey, an indication of Ag NP formation. The as-synthesized Ag NPs/CS-Starch bio-composite was retrieved by centrifugation and washed well with DI-water followed by drying at 40 °C.

## 2.2. Assessment of antioxidant capacity

The Ag NPs/CS-Starch bio-nanocomposite in 11 variable concentrations (1-1000 µg/ml, 1 ml each) was introduced to DPPH methanolic solution (1ml, 300 µM) and the total volume of the mixture was made up to 4000 µl with MeOH. Subsequently, the falcons were vortexed and remained in dark for 30 min. Finally, the color change due to radical quenching was monitored spectrophotometrically at a wavelength of 517 nm. The scavenging capacity of DPPH radical expressed in terms of % inhibition was determined by the following equation:

$$I (\%) = (A_0 - A_S) / A_0 \times 100$$

Where, A<sub>0</sub> is the absorption of the control (containing all reactive components without sample and A<sub>S</sub> is the absorption of the sample) [13,14].

## 2.3. Assessment of cytotoxicity by MTT protocol

The leukemia cancer cells (acute myeloid leukemia (32D-FLT3-ITD and Human HL-60/vcr), acute lymphoblastic leukemia (MOLT-3 and TALL-104), and acute T cell leukemia (Jurkat, Clone E6-1 and J.RT3-T3.5)) were used in this study.

Cancer cell lines were placed in 1640-RPMI medium from Gibco manufacturer and were cultured after adding 10% bovine serum, 1% streptomycin and penicillin antibiotics and 2% glutamine. At this stage, the cell culture flasks were kept in an incubator with 5% CO<sub>2</sub> and 95% humidity at a temperature of 37degC, and the culture medium was replaced every three days. In this step, flasks with 80% cell density were used (flasks filled with cells up to 80% of the bottom). First, the culture medium was removed from the surface of the cells and by adding 1 ml of trypsin for 3 minutes and then adding the same volume of medium to neutralize the effect of trypsin, all the cells were separated from the flask bottom. This cell suspension was centrifuged at 1200 rpm for 4 minutes. The liquid above the sediment was discarded and 1 ml of culture medium was added to the sediment. By taking 10 µl of the cell suspension and adding the same amount of trypan blue on the surface of the neobar slide, the number of living cells was counted. The number of 10,000 cells from this cell suspension was added to each well of 96-well plates and 180 µl of culture medium was added to it. In the next step, 20 µl different concentrations of nanoparticles were added to the wells. In this research, based on the conventional concentrations of nanoparticles at the 0-1000 µg/ml, they were added to cancer cells. Another group of cells were tested as a control, without adding nanoparticles and only by adding water instead of nanoparticles, and each experiment was done in four replicates. After 24, 48 and 72 hours, the medium on the cells was replaced with a new medium. Then 20 µl MTT solution was added to each well and placed in a greenhouse for 4 hours in the dark in a CO<sub>2</sub> incubator. During this time, the mitochondrial succinate dehydrogenase enzyme of living cells changes the yellow MTT solution into purple formazan crystals, which are insoluble in water. In the next step, 200 µl of DMSO (Dimethylsulfoxide) was added to the empty medium and shaken for 20 minutes to dissolve the light-producing crystals. In the last step, the absorbance was read with a wavelength of 492 and then 630 nm in an ELISA reader. Finally, the percentage of cell viability was calculated after dividing the optical absorbance (OD) of treated cells compared to control cells and multiplying by 100 [13].

The findings were analyzed by SPSS-22 using independent t-test.

## 3. Results and Discussion

### 3.1. Analysis of characterization data of the bio-nanocomposite

The Ag NPs/CS-Starch bio-composite was synthesized following a stepwise post-synthetic modification approach. A hydrogel mixture of CS and starch biopolymers was used as the structure directing template or a sustainable machinery for the green synthesis of functionalized nanocomposite particle. The duo had the function of affording stability to the NPs. Nevertheless, after the synthesis we had the urge to characterize it using a range of advanced analytical techniques like FT-IR, SEM, TEM, EDX and XRD.

The hierarchical decoration of the particle could be monitored by FT-IR analysis. Fig. 1 depicts the compilation of FT-IR spectra of its precursors, CS, Starch, intermediate CS-Starch hydrogel and the final Ag NPs/CS-Starch material. Fig. 1a shows the typical vibrations of CS molecule, being found at  $1031\text{ cm}^{-1}$ ,  $1384\text{ cm}^{-1}$ ,  $1593\text{ cm}^{-1}$ ,  $1651\text{ cm}^{-1}$  and  $3350\text{-}3500\text{ cm}^{-1}$ , being attributed to C–N stretching, C–O stretching of CH<sub>2</sub>-OH linkage, N-H bending, C=O stretching of amide linkage, O-H and N-H stretching [14]. Similarly, starch also shows its characteristic peaks at  $3445\text{ cm}^{-1}$  (broad),  $1078\text{ cm}^{-1}$  and  $1658\text{ cm}^{-1}$  due to overlapped O-H stretching, alcoholic C–O stretching and O–H bending vibrations (Fig. 1b) [15]. Fig. 1c, representing the FT-IR spectrum of CS-Starch composite, is almost an assemblage of Fig. 1a and 1b, with just a slight shift in vibrations, indicating the successful mixing of both. The final spectrum of Ag NPs/CS-Starch nanocomposite is also a look alike of Fig. 1c with a small shifting of vibrational peaks at higher or lower regions (Fig. 1d). This shift is anticipated derived from strong interactions of *in situ* synthesized Ag NPs with the surface organofunctions of CS-Starch composite.

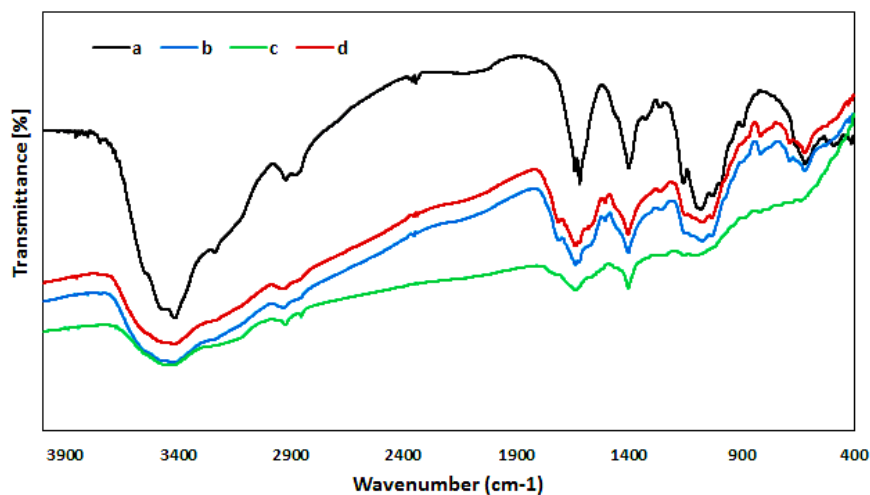


**Fig. 1.** FT-IR spectra of a) CS, b) Starch, c) CS-Starch and d) Ag NPs/CS-Starch bio-composite.

The particle morphology, size and shape of the Ag NPs/CS-Starch bio-composite was ascertained by the FE-SEM analysis. As shown in Fig. 2, It represents the dough of flour like appearance. However, no Ag nanoparticle like shaped things or its functional modification structure could be separately identified. Few pseudo-spherical shaped materials can be observed on close observation, characteristic to CS/starch hydrogel mixture. The particle seems to be agglomerated due to manual preparation of samples. However, more detailed insights of the particle structure was obtained from TEM analysis. Fig. 3 reveals the perfectly spherical shaped dark colored nanocomposite particles having dimension in the range of  $\sim 5\text{-}15\text{ nm}$ . The almost monodisperse particles are spread over the matrix without any sense of aggregation.

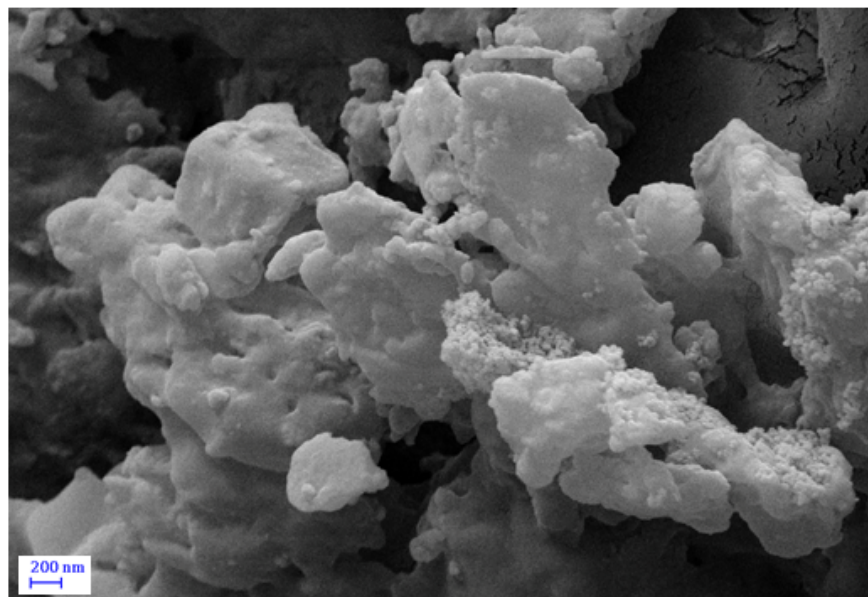


**Fig. 2.** FE-SEM image of the Ag NPs/CS-Starch bio-composite.

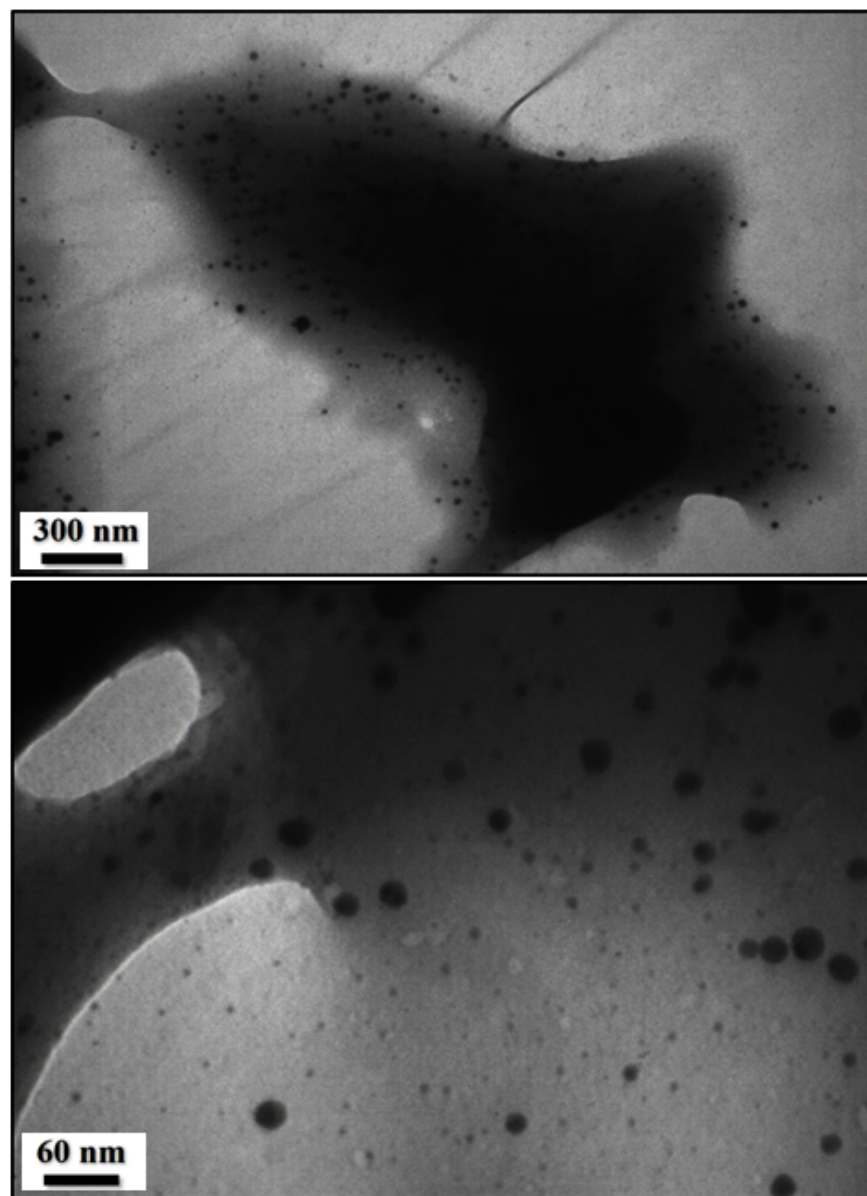


**Fig. 3.** TEM images of the Ag NPs/CS-Starch bio-composite.

Chemical constitution of the Ag NPs/CS-Starch nanocomposite was assessed by EDX analysis and the corresponding output is presented in Fig. 4. It clearly shows Au and Ag as the two metallic components along with some other peaks of C, N and O as the non-metals. A major signal of Au is observed at 2.1 KeV, which however not coming from the sample, but attributed to the gold vapor deposition prior to sample analysis. Another signal of Ag is found at 2.95 keV. The non-metal signals correspond to the associated CS-Starch composite. The map sum spectrum, being studied from the EDX profile evidently tells the major constituent of the composite being carbon (75.2 wt%). Ag occupies as 8.5 wt % of the total composite. The EDX data was further emphasized by elemental mapping analysis. On X-ray scanning of a section of FE-SEM image, the elemental constitution map or location can be detected. As can be seen from Fig. 5, the output displays a homogeneous distribution of constitutional elements over the surface. This is very important for the biocomposite for superior performance towards its applications.

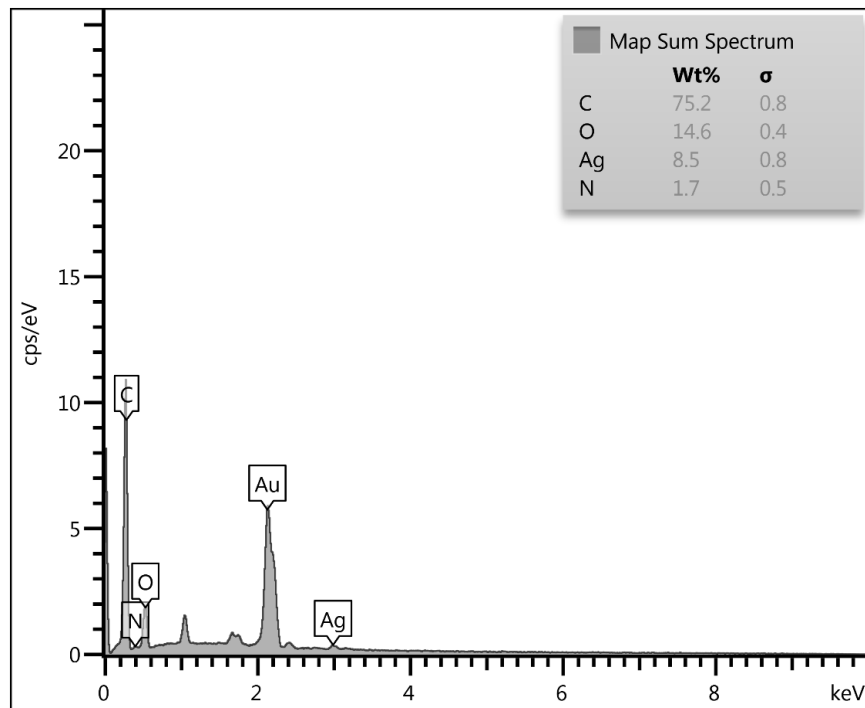


**Fig. 4.** EDX spectrum of the Ag NPs/CS-Starch bio-composite.

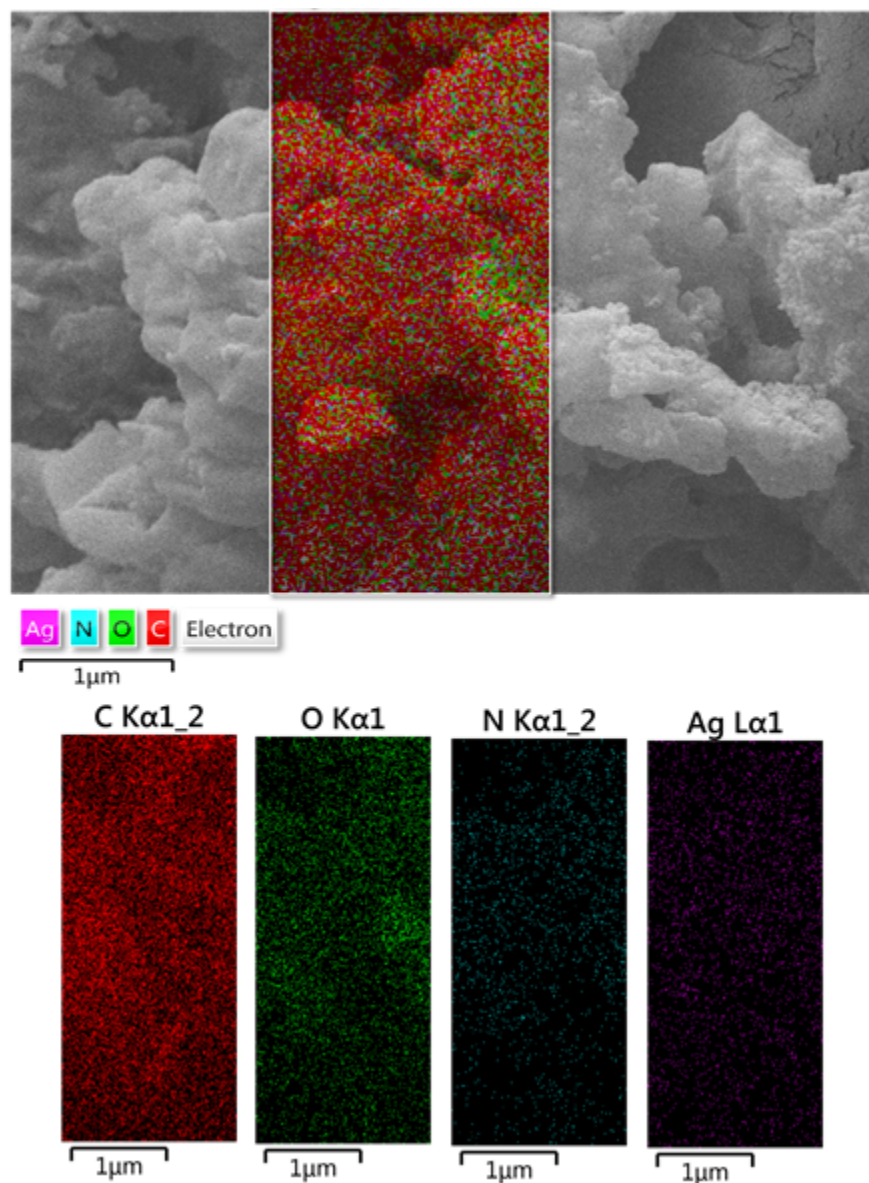


**Fig. 5.** Elemental mapping of Ag NPs/CS-Starch bio-composite.

The crystalline nature, phase behavior and purity of the Ag NPs/CS-Starch nanocomposite was ascertained by XRD investigations. A broad diffraction signal found in Fig. 6 in the  $2\theta$  region up to  $2\theta = 20^\circ$  was contributed from poorly crystalline CS-Starch composite. The further region is however fairly crystalline, attributed to Ag *fcc* unit cell. It displays the characteristic Bragg's diffraction peaks at  $2\theta = 38.4^\circ$ ,  $44.5^\circ$ ,  $65.2^\circ$  and  $78.1^\circ$  related to the Ag *fcc* (111), (200), (220) and (311) crystalline planes. These signals resemble closely to the standard (JCPDS No.87-0717).

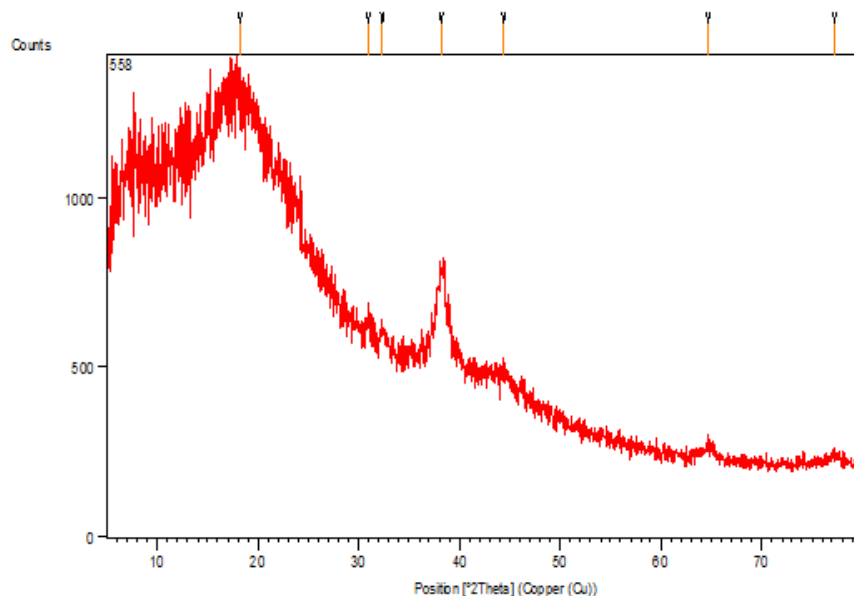


**Fig. 6.** XRD pattern of the Ag NPs/CS-Starch bio-composite.

### 3.2. The biological application of Ag NPs/CS-Starch bio-nanocomposite

A living cell is a collection of microscopic components with specific functions and functions. The plasma membrane surrounds the cell contents and is in contact with the external environment. The selective permeability of the membrane maintains the stability of the cell with the help of various transport mechanisms [15-18]. Small-sized nanoparticles easily pass through the membrane and due to their special surface properties, they interact with important cellular components such as mitochondria, lysosomes, and nuclei. The continuity of the structure and maintenance of the function of cells is often determined by biological macromolecules such as carbohydrates, lipids, and proteins. The structure of biomolecules changes under the influence of interaction with various types of nanoparticles [19,20].

Molecular oxygen dissolved in biological fluids is transformed into singlet oxygen under the influence of light energy required for biological transfer reactions. Superoxide radical is formed by a reduction reaction of oxygen molecule. This reaction can be done as a result of the redox cycle, or enzymatically with the catalysis of NADPH oxidase, and also as a byproduct of enzymatic reactions with Xanthine oxidase and a byproduct of the electron transport chain in mitochondria [20-23]. By upregulating the xanthine oxidase and NADPH oxidase enzymes, nanomaterials increase the production of superoxide radicals in some cells such as macrophages and neutrophils and trigger inflammatory reactions. The superoxide anion is suddenly converted to hydrogen peroxide ( $H_2O_2$ ) by the catalysis of the superoxide dismutase enzyme and with the help of copper, manganese or zinc as a cofactor. The dissolution of nanomaterials based on iron or copper catalyzes the formation of active oxygen species and through the Fenton reaction leads to the production of hydroxyl (OH) and peroxy (OOH) free radicals [24,25]. For example,  $TiO_2$  nanoparticles used in sunscreens produce singlet oxygen and superoxide under the influence of light rays. An increase in the level of ROS leads to inflammatory responses such as an increase in cells with polymorphous nuclei and disturbances in the phagocytosis process of macrophages in some model animals such as rodents [21-25]. Oxidative stress is caused by the predominance of free radicals on antioxidants and is one of the main mechanisms of toxicity of most metal nanoparticles such as gold, zinc oxide, and silver. Oxidative stress by regulating redox-sensitive transcription factors, activates some kinase enzymes and intermediate proteins of inflammatory reactions and causes tissue damage such as damage to the cell membrane, genetic material and biological macromolecules

[18-22]. At very high levels, disruption of the signaling pathways inside the cell leads to apoptosis and cell necrosis. Reactive oxygen species disrupt the function of the central nervous system by peroxidizing the unsaturated fatty acids of neuronal cells. Clogging of blood vessels, blood pressure and re-narrowing of arteries after angioplasty due to ROS cause disorders of the cardiovascular system. Mitochondria are one of the ROS production main sources through the electron transport respiratory chain [19-21]. Several clinical syndromes such as stroke, Duchenne muscular dystrophy, cardiac conduction defects due to ROS oxidative attack and mitochondrial DNA double-strand break occur. By producing reactive oxygen species in cancer cells, nanoparticles create changes in the chemical structure of histones or other proteins that are effective in shaping the structure of DNA [23-25]. Unfolding of the helical structure of DNA disrupts gene expression and malfunction of regulation of cellular function of cancer cells. In addition to ROS toxicity, some nanoparticles use other effective mechanisms for cell damage by releasing metal ions, accumulating in some cellular components, and interacting with nuclear components. In general, the cell damage mechanisms by nanoparticles include (1) membranes physical damage (2) Structural changes in the cell skeleton components (3) Disturbance in oxidative and transcription damage (4) Mitochondria damage (5) Dysfunction of lysosome (6) ROS production (7) Membrane proteins dysfunction (8) Mediators and inflammatory factors synthesis [19-25].

Herein, the antioxidant potential of Ag NPs/CS-Starch nanocomposite was assessed by DPPH radical scavenging capacity and the results is expressed in terms of percentage inhibition. This is displayed in Fig. 7. The data output at different sample concentrations were compared to BHT as the reference compound. In the corresponding analysis, the  $IC_{50}$  of Ag NPs/CS-Starch nanocomposite and BHT against DPPH free radicals were 314 and 125  $\mu\text{g}/\text{mL}$ , respectively.

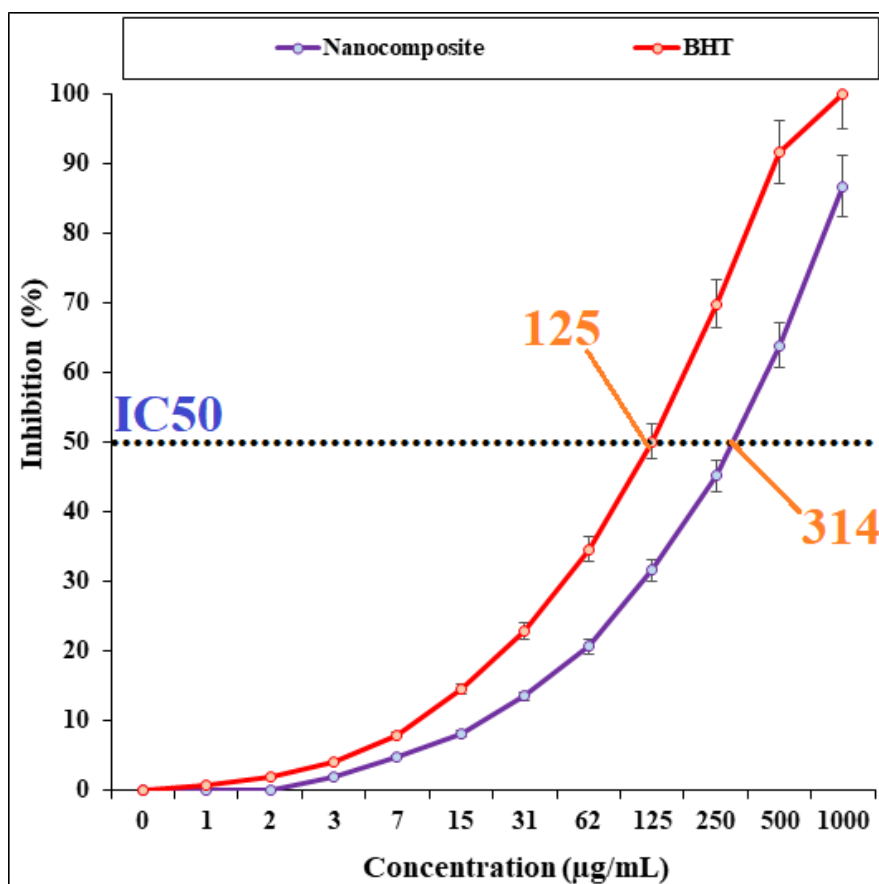


**Fig. 7.** The antioxidant properties of nanocomposite and BHT against DPPH.

Furthermore, in the cytotoxic assays following MTT study the experimental nanosample was treated to different leukemia cell lines at several concentrations. The analysis was done for 48 h against acute myeloid leukemia (32D-FLT3-ITD and Human HL-60/vcr), acute lymphoblastic leukemia (MOLT-3 and TALL-104), and acute T cell leukemia (Jurkat, Clone E6-1 and J.RT3-T3.5) cell lines (Figures 8-10). The material is safe to the normal cell line, HUVEC, and remains unaffected, being showed in Fig. 11. Interestingly, the % cell viability of malignant leukemic cell lines against the nano-formulated drug reduced with increasing concentrations or doses. The yellow colored MTT solution gets reduced to purple colored formazan crystal which is measured spectrophotometrically at 570 nm. The corresponding IC<sub>50</sub> values in the MTT assay against the cell lines were observed as 203, 301, 250, 227 and 102, 193 respectively.

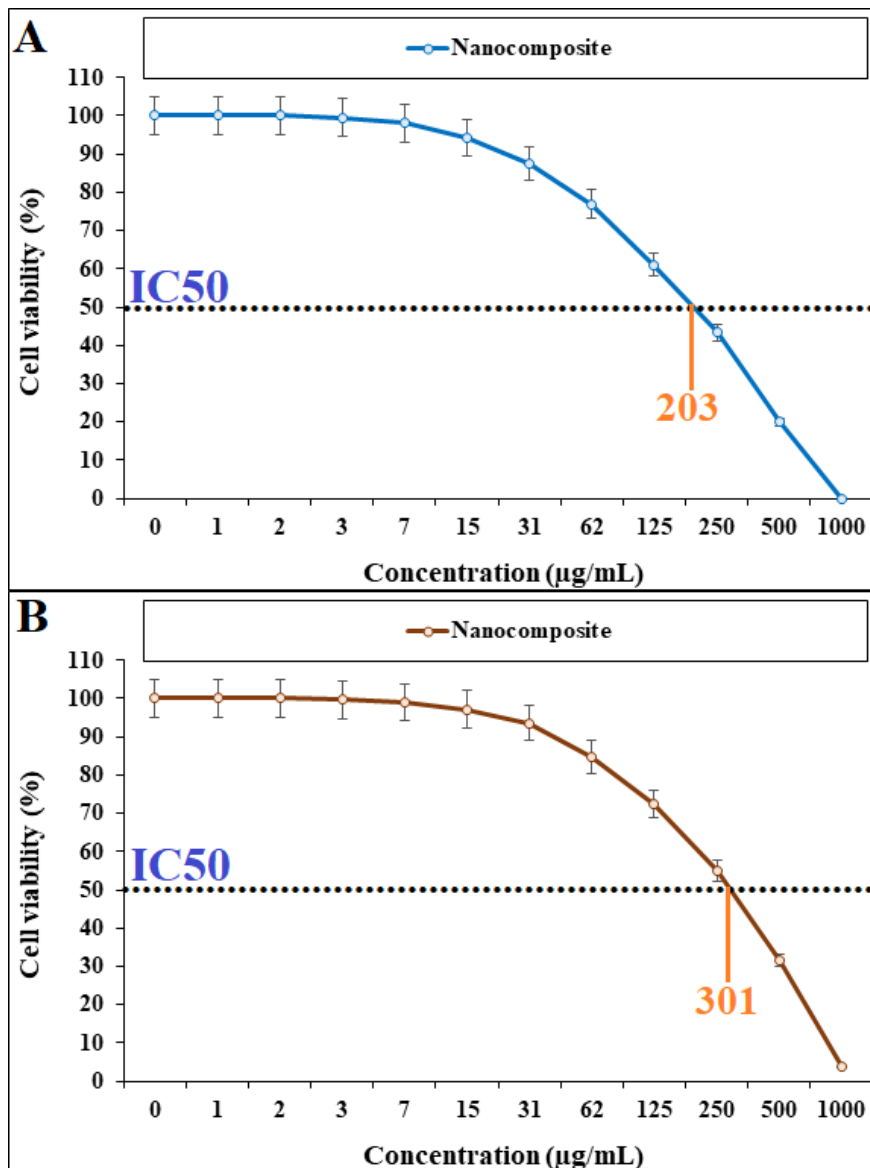


**Fig. 8.** The anti-leukemia properties of nanocomposite against 32D-FLT3-ITD (A) and Human HL-60/vcr (B) cell lines.

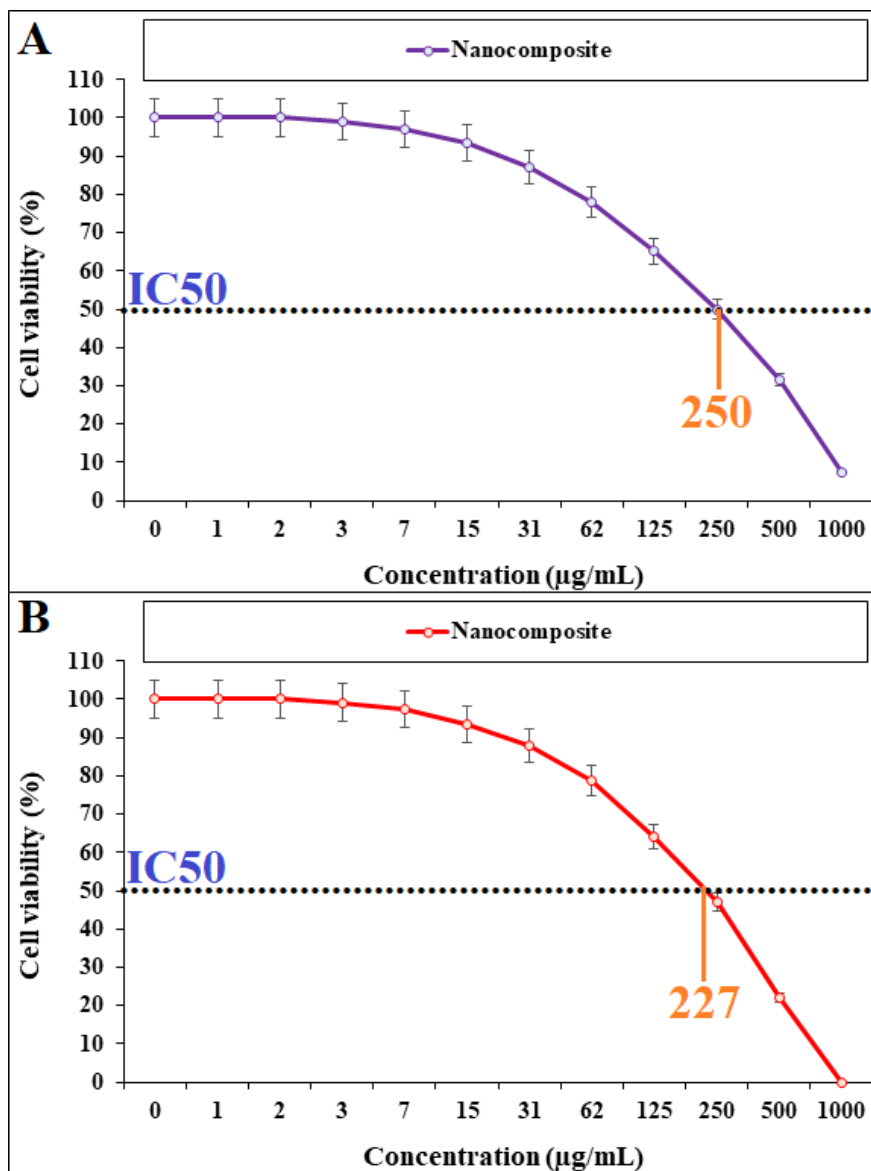


**Fig. 9.** The anti-leukemia properties of nanocomposite against MOLT-3 (A) and TALL-104 (B) cell lines.

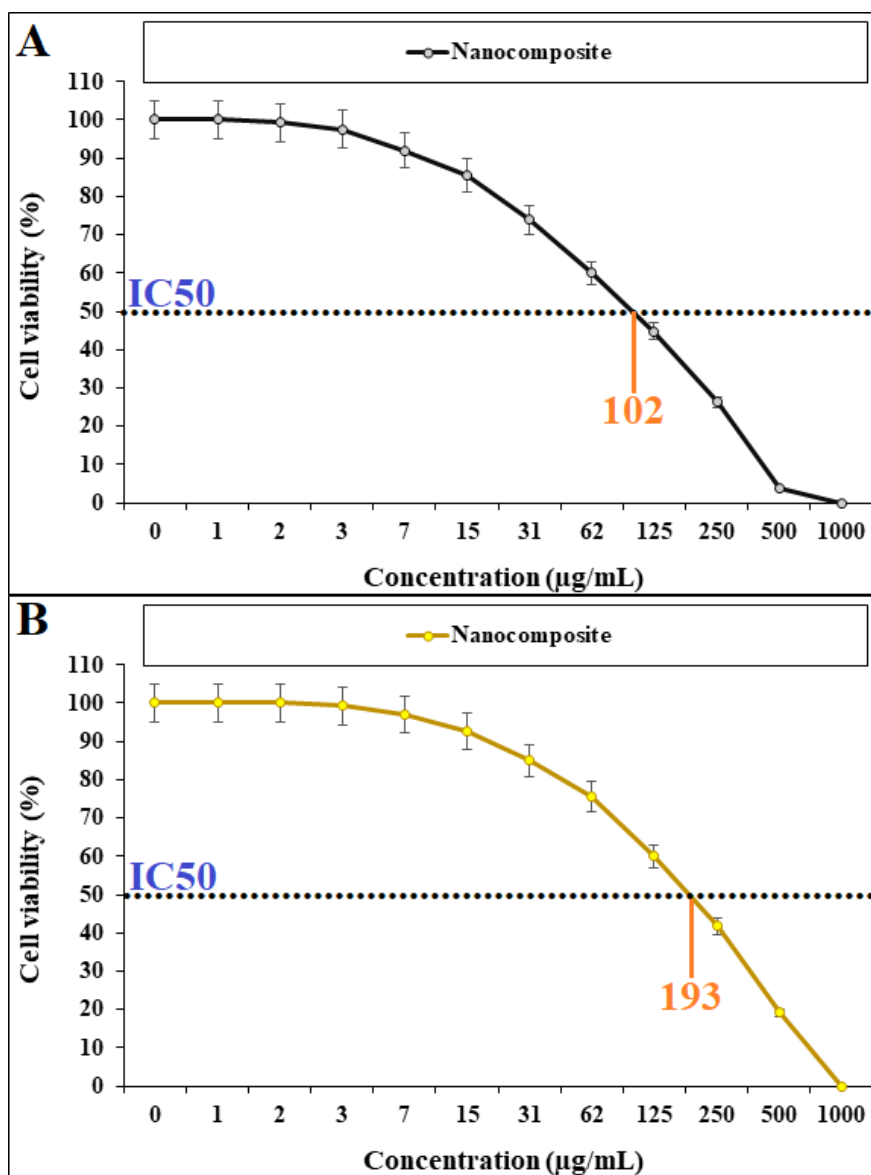


**Fig. 10.** The anti-leukemia properties of nanocomposite against Jurkat, Clone E6-1 (A) and J.RT3-T3.5 (B) cell lines.

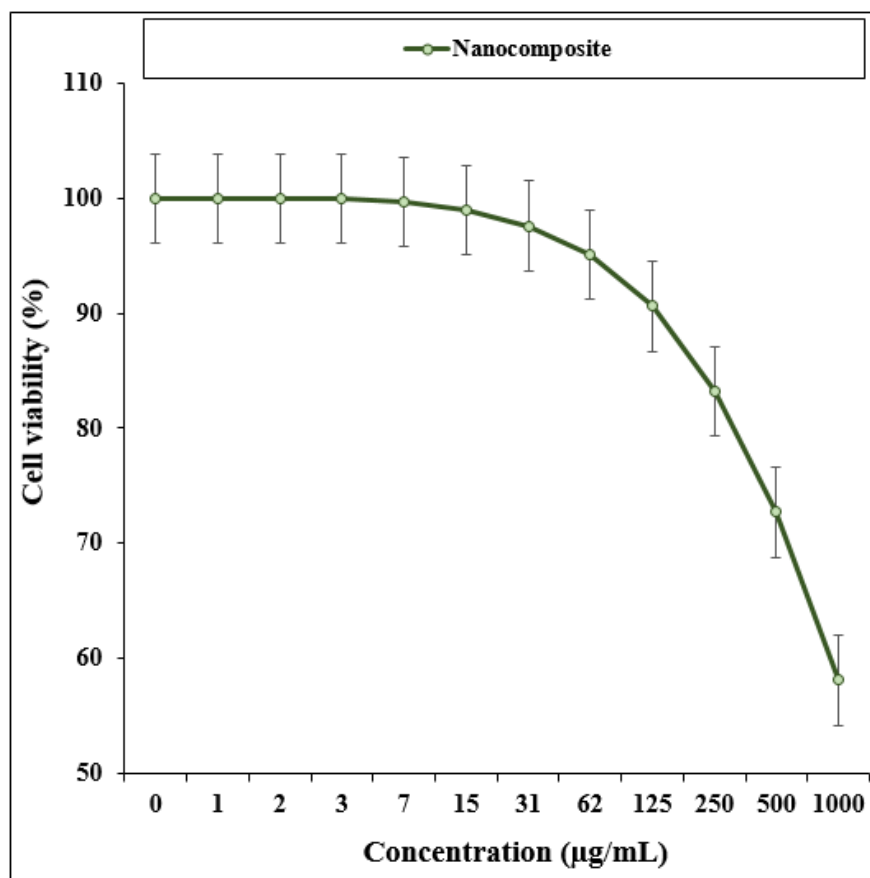


**Fig. 11.** The cytotoxicity effects of nanocomposite against normal (HUVEC) cell line.

#### 4. Conclusions

In summary, we have represented a bio-inspired method for the synthesis of stable Ag NPs being encapsulated and stabilized over pre-designed chitosan-starch bio-composite hydrogel. The procedure involved sustainable protocols and free from any hazardous and toxic chemicals. The material was analyzed towards its physicochemical characterizations following a wide range of technical methods. The Ag NPs formed were almost monodisperse in dimension in the range of 5-15 nm. They are uniformly distributed without any aggregations. The material was directed in the bio-analysis for antioxidant studies and its efficiency in the inhibition of different kinds of leukemia cell lines. In the antioxidant study the material in different concentration was investigated to quench the DPPH free radicals and was found to produce outstanding results. Again, the cytotoxicity analysis by MTT assay over the 6 leukemia cell lines were also carried out at different sample concentrations. The % cell viability of the same was found to decrease dose-dependently. However, the normal cell lines was found to be unaffected in the same study. This justifies the Ag NPs/CS-Starch nanocomposite could be considered as a competent nano-formulated drug candidate against different leukemia cancers. Further research on this study would be greatful in discovering a new dimension in the cancer research.

#### Disclosure statement

No potential conflict of interest was reported by the authors.

#### Data Availability Statement

The data that support the findings of this study are available from the corresponding author, [author initials], upon reasonable request.

## References

1. Kolosnjaj-Tabi J., di Corato R., Lartigue L., Marango I., Guardia P., Silva A.K., Luciani N., Clément O., Flaud P., Singh J.V., et al. Heat-generating iron oxide nanocubes: Subtle “destructorators” of the tumoral microenvironment. *ACS Nano*. 2014;8:4268–4283.
2. Maier-Hauff K., Ulrich F., Nestler D., Niehoff H., Wust P., Thiesen B., Orawa H., Budach V., Jordan A. Efficacy and safety of intratumoral thermotherapy using magnetic iron-oxide nanoparticles combined with external beam radiotherapy on patients with recurrent glioblastoma multiforme. *J. Neurooncol*. 2011;103:317–324.
3. Laurent S., Dutz S., Häfeli U.O., Mahmoudi M. Magnetic fluid hyperthermia: Focus on superparamagnetic iron oxide nanoparticles. *Adv. Colloid Interface Sci*. 2011;166:8–23.
4. Danhier F., Feron O., Preat V. To exploit the tumor microenvironment: Passive and active tumor targeting of nanocarriers for anti-cancer drug delivery. *J. Control Release*. 2010;148:135–146.
5. Caputo F., de Nicola M., Ghibelli L. Pharmacological potential of bioactive engineered nanomaterials. *Biochem. Pharmacol*. 2014;92:112–130.
6. Van Landeghem F.K., Maier-Hauff K., Jordan A., Hoffmann K.-T., Gneveckow U., Scholz R., Thiesen B., Brück W., von Deimling A. Post-mortem studies in glioblastoma patients treated with thermotherapy using magnetic nanoparticles. *Biomaterials*. 2009;30:52–57.
7. Orel V., Shevchenko A., Romanov A., Tselepi M., Mitrelias T., Barnes C.H., Burlaka A., Lukin S., Shchepotin I. Magnetic properties and antitumor effect of anocomplexes of iron oxide and doxorubicin. *Nanomedicine*. 2015;11:47–55.
8. Hilger I., Kaiser W.A. Iron oxide-based nanostructures for MRI and magnetic hyperthermia. *Nanomedicine*. 2012;7:1443–1459.
9. Bhattacharyya S., Kudgus R.A., Bhattacharya R., Mukherjee P. Inorganic nanoparticles in cancer therapy. *Pharm Res*. 2011;28:237–259.
10. Silva A.C., Oliveira T.R., Mamani J.B., Malheiros S.M., Malavolta L., Pavon L.F., Sibov T.T., Amaro E., Jr., Tannus A., Vidoto E.L. Application of hyperthermia induced by superparamagnetic iron oxide nanoparticles in glioma treatment. *Int. J. Nanomed*. 2011;6:591–603.
11. Johannsen M., Thiesen B., Wust P., Jordan A. Magnetic nanoparticle hyperthermia for prostate cancer. *Int. J. Hyperthermia*. 2010;26:790–795.
12. (a) Hemmati S *et al* . *Appl Organometal Chem*2019; 33: e5277. DOI:10.1002/aoc.5277. (b) Hemmati S *et al* . *Appl Organometal Chem*2020; 34: e5274. DOI:10.1002/aoc.5274. (c) Zangeneh MM. *Appl Organometal Chem*2020; 34: e5295. DOI:10.1002/aoc.5295. (d) Zangeneh MM *et al* . *Appl Organometal Chem* 2019; 33: e4961. (e) Zangeneh MM *et al* . *Appl Organometal Chem*. 2019, 33, e5016. (f) Zangeneh A *et al* . *Appl Organometal Chem*. 2019,33, e5247. DOI:10.1002/aoc.5247. (g) Zangeneh MM *et al* . *Appl Organometal Chem* 2019; 33: e5246. DOI: 10.1002/aoc.5246. (h) Mahdavi B *et al* . *Appl Organometal Chem* 2019; 33: e5248. DOI:10.1002/aoc.5248.
13. (a) Hamelian M *et al* . *Appl Organometal Chem* 2018; 32: e4458. (b) Hemmati S *et al* . *Polyhedron* 2019; 158: 8-14. (c) Hamelian M *et al* . *Appl Organometal Chem* 2020; 34: e5278. (d) Mohammadi G *et al* . *Appl Organometal Chem*2020; 34: e5136. (e) Ahmada A *et al* . *Appl Organometal Chem* 2020; 34: e5378. (f) Zangeneh MM. *Appl Organometal Chem* 2020; 34: e5295. (g) Jalalvand AR *et al* . *J Photochem Photobiol B* 2019; 192: 103–112.
14. R. Fazaeli, H. Aliyan, N. Fazaeli, *Open Catal. J.* 3 (2010) 14–18.

15. S. R. Konda, B. R. Reguri, M. Kagga, *Der Pharma Chem.* 6 (2014) 228–233.
16. C. Pan, B. Hu, W. Li, Y. Sun, H. Ye, X. Zeng, *J. Mol. Catal. B: Enzym.* 61 (2009) 208–215.
17. C. Sartori, D. S. Finch, B. Ralph, *Polymer* . 38 (1997) 43-51.
18. Felice B., Prabhakaran M.P., Rodríguez A.P., Ramakrishna S. Drug delivery vehicles on a nano-engineering perspective. *Mater. Sci. Eng. C.* 2014;41:178–195.
19. Fernandes E., Ferreira J.A., Peixoto A., Lima L., Barroso S., Sarmento B., Santos L.L. New trends in guided nanotherapies for digestive cancers: A systemic review. *J. Control Release.* 2015;209:288–307.
20. Caputo F., de Nicola M., Ghibelli L. Pharmacological potential of bioactive engineered nanomaterials. *Biochem. Pharmacol.* 2014;92:112–130.
21. Danhier F., Feron O., Preat V. To exploit the tumor microenvironment: Passive and active tumor targeting of nanocarriers for anti-cancer drug delivery. *J. Control Release.* 2010;148:135–146.
22. Laurent S., Dutz S., Häfeli U.O., Mahmoudi M. Magnetic fluid hyperthermia: Focus on superparamagnetic iron oxide nanoparticles. *Adv. Colloid Interface Sci.* 2011;166:8–23.
23. Maier-Hauff K., Ulrich F., Nestler D., Niehoff H., Wust P., Thiesen B., Orawa H., Budach V., Jordan A. Efficacy and safety of intratumoral thermotherapy using magnetic iron-oxide nanoparticles combined with external beam radiotherapy on patients with recurrent glioblastoma multiforme. *J. Neurooncol.* 2011;103:317–324.
24. Kolosnjaj-Tabi J., di Corato R., Lartigue L., Marango I., Guardia P., Silva A.K., Luciani N., Clément O., Flaud P., Singh J.V., et al. Heat-generating iron oxide nanocubes: Subtle “destructorators” of the tumoral microenvironment. *ACS Nano.* 2014;8:4268–4283.
25. Bhattacharyya S., Kudgus R.A., Bhattacharya R., Mukherjee P. Inorganic nanoparticles in cancer therapy. *Pharm Res.* 2011;28:237–259.